Compressive Yield Stress of Flocculated Suspensions: Determination via Experiment

Matthew D. Green
Dept. of Chemical Engineering

Maria Eberl and Kerry A. Landman
Dept. of Mathematics

Advanced Mineral Products Centre, University of Melbourne, Parkville, Victoria 3052, Australia

The compressive yield stress $P_y(\phi)$ is an extremely useful parameter for the characterization of concentrated flocculated suspensions. It is a measure of the strength of interparticle bonds in a networked suspension structure and is used in process design and control of mineral colloidal suspension dewatering. Previous work developed a method for determining this compressive yield stress via the equilibrium sediment height technique using a centrifuge. Here justification for a simple approximate technique to obtain $P_y(\phi)$ is discussed. A new more accurate iterative algorithm is also described. By generating synthetic data, where the exact $P_y(\phi)$ is known, the accuracy of the two techniques can be evaluated properly for the first time. The relative merits and failings of the techniques are discussed. An example is given to show how these techniques work on real experimental data.

Introduction

The production of concentrated mineral or colloidal suspensions is a vital stage in many industrial processes. Superthickeners and deep cone thickeners have made a particular impact in environmental waste minimization in the alumina industry. Compressional rheology plays an important role in the design and control of solid-liquid separation processes.

Traditional dewatering processes have three distinct regions (Coe and Clevenger, 1916): a clear liquid region; a hindered settling region in which the concentration is relatively constant with height and particles interfere with each other during their descent; and finally a compression region where a concentration gradient exists in which each floc is in mutual contact and compression of the structure occurs due to the weight of the overlying sediment or from the application of external pressure. Highly concentrated suspensions may be produced from the compression region in thickening operations such as continuous gravity thickeners, centrifugal thickeners, batch thickeners, and pressure filtration devices. Efficient operation of these dewatering processes to produce a highly concentrated and easily processed product requires a good understanding of the compression rheology of the concentrated flocculated suspensions involved.

To characterize the compressional rheology of concentrated flocculated suspensions, the compressive yield stress for the suspension needs to be determined. One such technique is to measure the solids concentration profile of a suspension sample that has been centrifuged to equilibrium. This can be done using a sophisticated X-ray or γ-ray device such as that used by Bergström et al. (1992a) or less elegantly by taking cuts of the sample and measuring the solids concentration of each cut. The compressive yield stress curve can then be determined via a simple integration. Another technique involves measuring the final height of a filter cake after filtration at different constant pressures (Landman et al., 1995). This method successfully predicted filtration rates and cake density in a kaolin plant filter (Eberl et al., 1995). A third common experimental technique accepted in engineering practice simply involves measuring the equilibrium sediment

Correspondence concerning this article should be addressed to K. A. Landman.

height of the suspension after rotation in a centrifuge at different speeds (De Guingand, 1986; Green and Boger, 1992; Green et al., 1992). Consistency of the resulting compressive yield stress between these various experimental techniques is currently under investigation by Miller et al. (1995) and by our group.

This article is devoted to the equilibrium sediment height technique and the difficulties in determining the compressive yield stress from the raw data. Several methods may be used, including an approximation method which until now has been used with little justification and a new (exact) iterative algorithm. These two methods are described and compared in detail, and difficulties associated with them are outlined.

In order to know how accurate these methods are for finding the "true" $P_y(\phi)$ for a flocculated suspension, we generated synthetic raw equilibrium height data from several chosen $P_y(\phi)$ forms. This data was used as input to our algorithms to obtain a compressive yield stress function. These determined functions were then compared to the true function. Only such an analysis gives a true picture of the accuracy of the various algorithms.

This article provides the necessary validation of a technique already being used in engineering practice and currently being introduced to the alumina and kaolin industries; it also shows why the generally accepted approximation method is comparatively accurate and how to implement a more accurate iterative technique if that is required.

Suspension Structure

The exact nature of the compression region for flocculated suspensions needs to be defined. Many studies (Dixon, 1978; Kos, 1977; Michaels and Bolger, 1962; Tadros, 1985, 1986; Buscall et al., 1987) have been made which attempt to microscopically describe the compression region and the mechanism acting therein to increase the solids concentration. In a consolidating system of flocculated particles, a concentration exists called the gel point ϕ_g, above which the suspension enters the compression region. The particles in the compression region are subject to a wide range of interparticle forces depending upon the nature and degree of the flocculation; a networked structure is formed which has a dramatically altered rheology. In this structure, particles experience compressive forces due to the network pressure from the weight of the overlying sediment. This compressive force is transmitted downwards throughout the continuous linked structure. Collapse of the structure is resisted by the strength of the interparticle bonding and also by the upward drag force of the expelled liquid through the structure. This drag explains the slow collapse over a period of time of the structure (Dixon, 1978), as the applied stress does not act immediately throughout the structure because it is partly balanced by the liquid drag. After sufficient time, the suspension will eventually reach an equilibrium condition with all forces balanced and no further consolidation occurring. [As usual (Bergström, 1992b; Landman et al., 1988), the inertial forces, bulk and wall shear forces can be neglected in comparison to the forces discussed here.]

With flocculated suspensions, a local particle pressure P_p is generated due to direct interactions between suspended particles. Even though P_p is conventionally termed pressure, P_p is really the zz component of the stress tensor, where z is the vertical coordinate. This characterizes the resistance of the network to uniaxial compression.

Once the particle volume fraction exceeds the gel point ϕ_g, a continuous network is formed. Compressive forces can be transmitted via the network throughout the structure which can then support itself. In this case, P_p should be thought of as a network pressure. If P_p is sufficiently small, the network will resist compression. As the applied compressive force (such as applied pressure via a piston or gravitational force with a centrifuge) is increased, a point will be reached where the network will no longer be able to resist elastically. Instead, the network will yield and irreversibly consolidate. This is due to the breaking or rearranging of bonds between particles and/or the formation of more contact points between particles. This process can be modeled by introducing the concept of the network possessing a compressive yield stress, $P_y(\phi)$, a function of the local volume fraction (Landman et al., 1988). $P_y(\phi)$ can be expected to depend implicitly on the properties of the network, such as the strength of interparticle bonds and the shear and compression history of the system. $P_y(\phi)$ can be expected to be an increasing function of ϕ, will be zero for $\phi \le \phi_g$, and will be very large for $\phi \to \phi_{cp}$, the close packing limit. Measurement of this function is essential for the full characterization and comparison of suspension systems.

The concentration profile of a sediment structure collapsing under compressional forces varies with time. This is illustrated in Figure 1 which shows the variation of the solids concentration with height in a fully structured batch suspension (i.e., has a uniform initial concentration $\phi_o > \phi_g$). Here z is the vertical distance from the thickener base, and $H(t)$ is the sediment height which decreases from the initial value H_o to the final equilibrium value H_{eq}. The solids concentration $\phi(z,t)$ and the compressive stress $P_y(z,t)$ vary with both position and time.

At any time in a collapsing structure, a critical height $z_c(t)$ (m) exists where the compressive force is equal to the total upward force made up of the network's resistive force and the liquid drag force. As illustrated in Figure 1, $z_c(t)$ divides the compression region into two subregions:

(1) Constant concentration plug at $z \ge z_c(t)$, where $\phi = \phi_o$

(2) Collapsing region at $z < z_c(t)$, where $\phi > \phi_o$.

Initially, the liquid drag is the dominant force due to the large amount of upflowing liquid, so that at $t = 0$, $z_c(t) = 0$ (i.e., the sediment is a constant concentration plug). As the

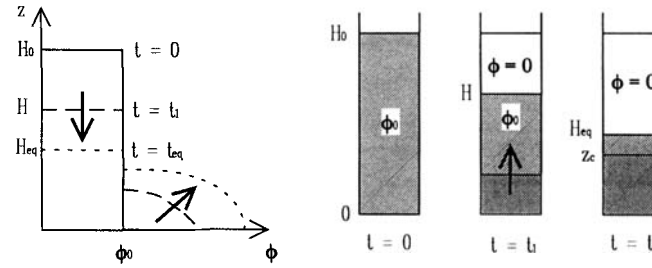

Figure 1. Variation of concentration with time for a sedimenting flocculated suspension in a centrifuge tube.

compression process continues, the contribution from the liquid drag decreases and $z_c(t)$ increases, usually passes through a maximum, then approaches H_{eq} at equilibrium but will never actually reach it.

For the compression mechanism to be fully exploited, a technique which enables the compression properties of a suspension to be measured and characterized is necessary. A mathematical framework has been developed by Buscall and White (1987) in which the consolidation behavior of concentrated flocculated suspensions is characterized by a parameter, the compressive yield stress $P_y(\phi)$. This parameter is assumed to be a function of the local concentration ϕ. $P_y(\phi)$ is defined by the following constitutive equation which describes the kinetics of collapse (Buscall and White, 1987)

$$\frac{D\phi}{Dt} = \begin{cases} 0, & P_p < P_y(\phi) \\ \kappa(\phi)[P_p - P_y(\phi)], & P_p \geq P_y(\phi), \end{cases} \tag{1}$$

where D/Dt is the material derivative and $\kappa(\phi)$ is a rate constant called the dynamic compressibility. Equation 1 says that the network resists compression if $P_p < P_y(\phi)$, but collapses if $P_p \geq P_y(\phi)$.

It can be argued that P_p will always be close to $P_y(\phi)$. If the drainage of the fluid is the rate determining step in the dynamics of collapse, then $\kappa(\phi)$ is of the order $O(\phi/\eta)$, where η is the fluid viscosity (Buscall and White, 1987). For this case, estimating the order of the terms in Eq. 1 gives

$$P_p = P_y(\phi)\left[1 - O\left(a_p^2/h_0^2\right)\right], \tag{2}$$

where a_p is the particle size and h_0 is the container size. Typically, $O(a_p^2/h_0^2) \sim (10^{-12} - 10^{-8})$, and therefore Eq. 1 can be replaced by

$$P_p(z,t) = P_y[\phi(z,t)], \tag{3}$$

in the compression zone. The compressive yield stress is thus a direct measure of the particle pressure or of the strength of the bonds between particles in a flocculated suspension under pressure.

It is important to note that the use of this equation assumes that compression is irreversible (since the pressure completely characterizes the local volume fraction), which is particularly important when viscoelastic systems are examined. This equation is also only strictly valid for fully flocculated systems possessing a contiguous space-filling network structure. Bergström (1992b) notes that for weakly flocculated systems in particular, the top portion of the sediment slowly increases in concentration, which is contrary to the model.

Determination of $P_y(\phi)$

The compressive yield stress function $P_y(\phi)$ can be obtained from centrifuge experiments (Buscall and White, 1987). Samples are placed in cylindrical, transparent, flat bottomed, centrifuge tubes and the equilibrium sediment height H_{eq} is measured for various increasing values of the gravitational acceleration g at the bottom of the tube. Initially, the volume fraction concentration of the flocculated suspension is uniform throughout at ϕ_0. Also required for the calculations are the initial height of the suspension H_0, the density difference between the solid and the fluid $\Delta\rho$, and the centrifuge radius from the center to the internal base of the tube R. These raw data are the basis of the so-called "equilibrium sediment height technique."

Starting with these raw (g, H_{eq}) data, equations governing the suspension mechanics produce a parameterization in g for $\phi(0)$ and $P(0)$; the volume fraction concentration and the pressure or solid stress at the bottom of the tube (at $z = 0$). [For simplicity, $P_p(z,t)$, which at equilibrium is independent of t, is now replaced by the notation $P(z)$.] Using these equations, $P(0)$ as a function of $\phi(0)$ can be calculated by an iterative or an approximate procedure that is described below. The application of Eq. 3 thus means that this curve is equivalent to the compressive yield stress curve $P_y(\phi)$.

Beginning with a force balance on a volume element of suspension and continuity equations on the solid and liquid phases, the underlying differential equation relating the pressure $P(z)$ to g at equilibrium may be determined

$$\frac{dP}{dz} = -\Delta\rho g\phi\left(1 - \frac{z}{R}\right). \tag{4}$$

This equation together with a mass conservation equation can be manipulated in various ways, as detailed in the Appendix. In so doing various functions are introduced, namely

$$Z(z) = \int_z^{H_{eq}}\left(1 - \frac{z}{R}\right)dz = (H_{eq} - z)\left(1 - \frac{H_{eq} + z}{2R}\right), \tag{5}$$

and ϵ and Δ, which are functions of g

$$\epsilon = \frac{1}{\phi_0 H_0 R}\int_0^{H_{eq}} \frac{dz\,\phi(z)}{(1 - z/R)^2}\left[Z(z) + \left(1 - \frac{H_{eq}}{R}\right)g\frac{dH_{eq}}{dg}\right], \tag{6}$$

$$\Delta = \frac{1}{R}\int_0^{H_{eq}} \frac{dzP(z)}{\Delta\rho g\phi_0 H_0(1 - z/R)^2}. \tag{7}$$

Then

$$\phi(0) = \frac{\phi_0 H_0(1 - \epsilon)}{\left(H_{eq} + g\dfrac{dH_{eq}}{dg}\right)\left(1 - \dfrac{H_{eq}}{R}\right) + \dfrac{H_{eq}^2}{2R}}, \tag{8}$$

$$P(0) = \Delta\rho g\phi_0 H_0(1 - \Delta), \tag{9}$$

which explicitly show how the ϵ and Δ functions act as corrections to $\phi(0)$ and $P(0)$, respectively. Note that when Δ is ignored, $P(0)$ represents the case when the gravitational force is constant throughout the sample (applicable to large-scale thickener operations and to pressure filtration).

The ϵ and Δ are integral functions of the concentration and pressure profiles in the centrifuge tube, and also involve H_{eq} and its derivative. These concentration and pressure profiles are unknown in the consolidating region $0 < z < z_c$; thus,

these functions must be solved by numerical integration together with the main differential equation, Eq. 4.

In the constant concentration zone $z_c < z < H_{eq}$

$$\phi = \phi_0$$

$$P(z) = \Delta\rho g\phi_0(H_{eq} - z)\left(1 - \frac{H_{eq} + z}{2R}\right), \tag{10}$$

using Eq. 4.

An alternate and more convenient method of solution is to solve associated differential equations. Now think of ϵ and Δ as functions of z, where $\epsilon(0) = 0$ and $\Delta(0) = 0$, such that

$$\frac{d\epsilon}{dz} = \frac{\phi\left[Z(z) + \left(1 - \frac{H_{eq}}{R}\right)g\frac{dH_{eq}}{dg}\right]}{\phi_0 H_0 R(1 - z/R)^2}, \tag{11}$$

$$\frac{d\Delta}{dz} = \frac{P(z)}{\Delta\rho\phi_0 H_0 gR(1 - z/R)^2}. \tag{12}$$

The ϵ and Δ in Eqs. 6 and 7 can now be thought of as the above functions evaluated at $\epsilon(H_{eq})$ and $\Delta(H_{eq})$. Using Eqs. 10 in the constant concentration zone, these correction terms become

$$\epsilon = \epsilon(H_{eq}) = \epsilon(z_c) + \frac{H_{eq} - z_c}{H_0 R(1 - z_c/R)}\left(\frac{H_{eq} - z_c}{2} + g\frac{dH_{eq}}{dg}\right), \tag{13}$$

$$\Delta = \Delta(H_{eq}) = \Delta(z_c) + \frac{g(H_{eq} - z_c)^2}{2H_0 R(1 - z_c/R)}, \tag{14}$$

so that Eqs. 4, 11 and 12 need only be integrated from $0 < z < z_c$ in order to calculate $\epsilon(z_c)$ and $\Delta(z_c)$. With ϵ and Δ found, these functions may now be used in Eqs. 8 and 9 to find $\phi(0)$ and $P(0)$ for each value of g.

Approximate Solution

An approximate solution can also be obtained using the mean value theorem (Buscall and White, 1987). From Eq. 4 evaluated at $z = 0$

$$\frac{1}{\phi(\xi)}\int_0^{P(0)} dP = \Delta\rho g H_{eq}\left(1 - \frac{H_{eq}}{2R}\right), \tag{15}$$

where $z = \xi$ such that $0 < \xi < z_c$ but is otherwise unknown. Hence,

$$P(0) = \Delta\rho g H_{eq}\phi(\xi)\left(1 - \frac{H_{eq}}{2R}\right). \tag{16}$$

Applying the mean value theorem to a conservation of mass equation gives

$$\phi(\xi')H_{eq} = \phi_0 H_0, \tag{17}$$

again for a value of ξ' between $0 < \xi' < z_c$.

If we assume that $\phi(\xi) = \phi(\xi')$, then Eqs. 16 and 17 yield

$$P(0) \approx \Delta\rho\phi_0 H_0 g\left(1 - \frac{H_{eq}}{2R}\right). \tag{18}$$

From Eq. A14 in the appendix this yields

$$\phi(0) \approx \frac{\phi_0 H_0\left[1 - \frac{1}{2R}\left(H_{eq} + g\frac{dH_{eq}}{dg}\right)\right]}{\left[\left(H_{eq} + g\frac{dH_{eq}}{dg}\right)\left(1 - \frac{H_{eq}}{R}\right) + \frac{H_{eq}^2}{2R}\right]}. \tag{19}$$

$P(0)$ and $\phi(0)$ may thus be directly calculated for each (g, H_{eq}) raw data point using the above two equations. Determination of the derivative dH_{eq}/dg at each point is all that is required.

The mean value "approximate" solution for $P(\phi(0))$ is a very good solution to the compression equations. This is demonstrated graphically in Figure 2 for a particular g value and for a particular synthetic function (discussed later). In Figure 2a the scaled concentration profile generated by the algorithm is shown. The equivalent "average" concentration $\phi(\xi')$ for that particular H_{eq} is indicated. In Figure 2b this value is used in the integral in Eq. 15, and this $P(0)/\phi(0)$ area is compared with the right side of the integral as calculated by the algorithm, which is the area under the curve. For the synthetic data tested, the relative error between the two calculations remained under 3% for a range of g values and synthetic functions, which is excellent given the relative simplicity of the solution. This verifies numerically that the approximate solution is sound.

Note that it does not appear possible to show theoretically that this simple solution is an accurate approximation for all functions $P_y(\phi)$.

Iterative Solution

The algorithm for the iterative solution is outlined in the flow chart in Figure 3.

Several points can be made regarding this procedure. First, to start the iterative solution, the initial guess for the $P(0)$ vs. $\phi(0)$ curve does not have to be the approximate solution. Alternatively, upper or lower bounds for $P(0)$ and $\phi(0)$ could be useful—it was found that the convergence rate was not affected.

During the numerical solution of the set of differential equations, a mass conservation check can also be performed by simultaneously integrating the differential equation,

$$\frac{dM}{dz} = \phi, \tag{20}$$

where M is the cumulative concentration of solids in the centrifuge tube.

Convergence of the solution can be achieved by checking that the difference between the sum of all Δs in successive

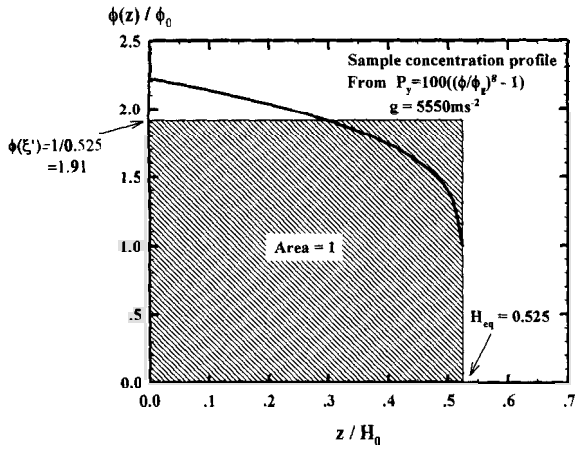

(a)

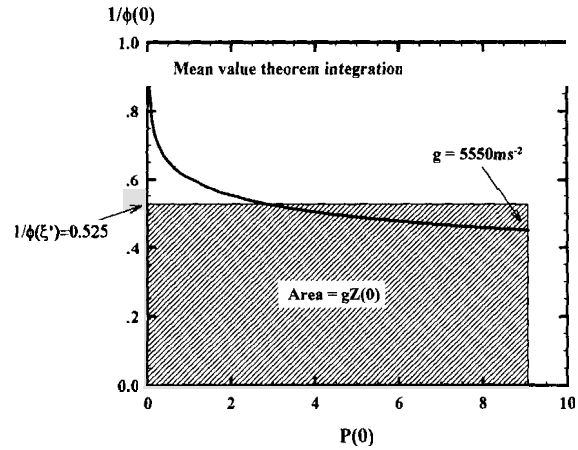

(b)

Figure 2. Numerical validation of the mean value theorem for the approximate solution.

(a) Sample concentration profile from an 8th-order power law function for $g = 5{,}550\ \text{ms}^{-2}$, showing the equivalent "average" concentration $\phi(\xi')$; (b) comparison of the $P(0)/\phi(0)$ areas as calculated by the algorithm and as by the mean value theorem (scaled units).

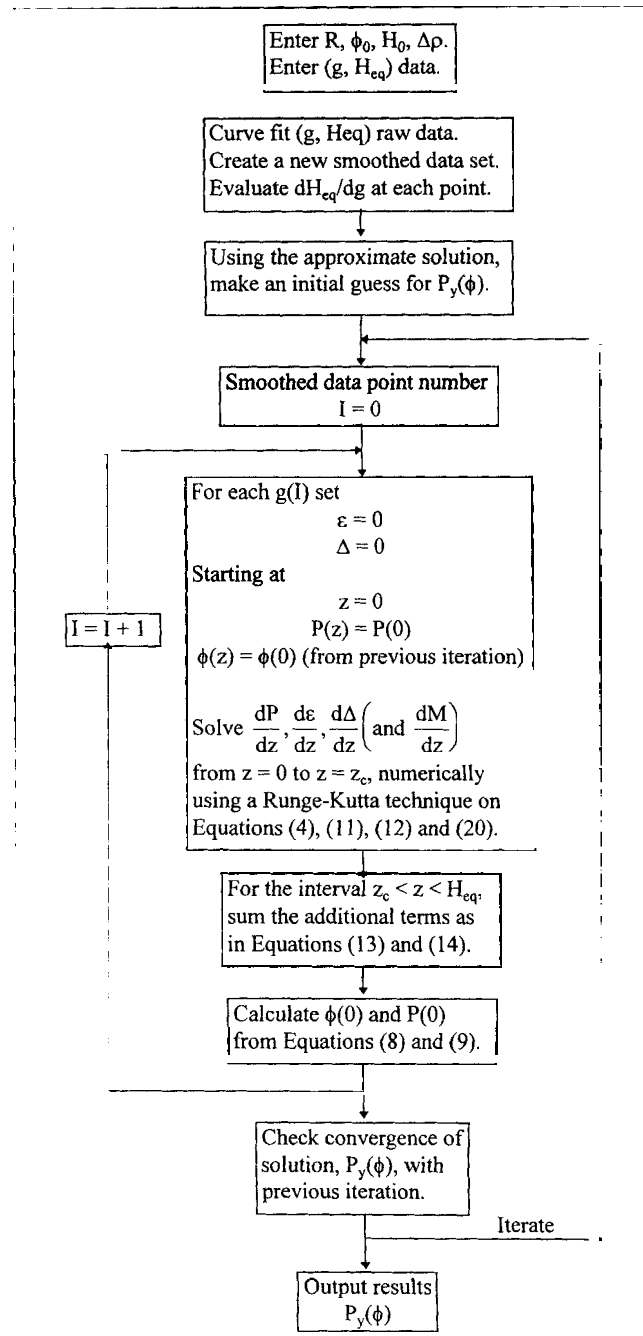

Figure 3. Iterative algorithm for the computation of the $P_y(\phi)$ curve from equilibrium sediment height data.

iterations is smaller than a specified tolerance, or some other appropriate convergence criterion.

A critical part of this algorithm is the accurate determination of the unknown z_c at which point the solution of the differential equations is halted. There are a number of techniques by which z_c can be estimated. The first involves the examination of the pressure curve in the constant concentration region $z_c < z < H_{eq}$ given by Eq. 10. This is a quadratic function in z and is a more slowly decreasing function of z than the $P(z)$ curve obtained from the numerical integration in the region $0 < z < z_c$. Hence, z_c can be determined by finding the point of intersection between these two curves, as is illustrated in Figure 4. In theory, at the point of intersection the two intersecting curves should possess the same slope thus giving a smooth, continuous pressure distribution. In practice, however, this is very difficult to achieve numerically and a certain tolerance is allowed.

The second stopping criterion that may be used to determine z_c is to look for the point where $\phi \le \phi_0$ since at this point, $\phi(z_c) = \phi_0$. For typical functions of $P(z)$, ϕ drops off steeply near $z = z_c$, especially for high g values. This will be demonstrated in later figures when concentration profiles for synthetic data are examined. The error in the calculated value of z_c is thus not significant if this criterion is not exactly met.

Other less accurate stopping criteria may also be used, especially in early iterations when the initial guess may be some way from the final solution. In order of decreasing accuracy, these check when $z \ge H_{eq}$ or $P(z) \le 0$.

The above algorithm differs from an earlier algorithm de-

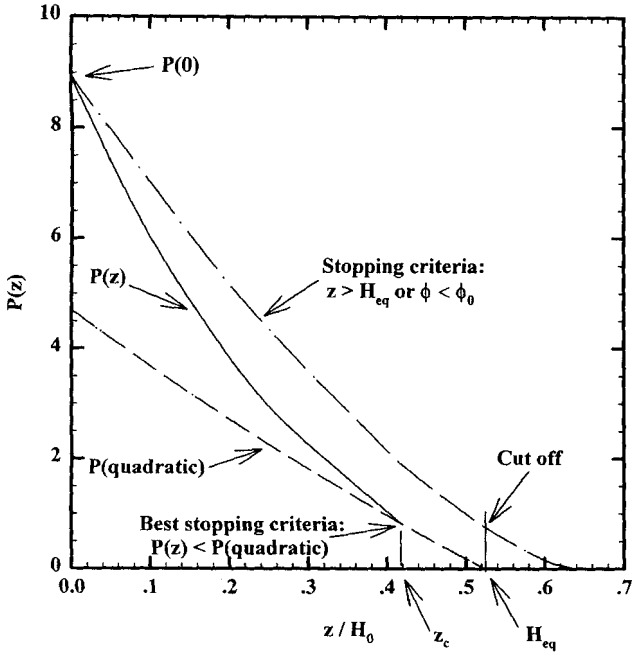

Figure 4. Stopping criteria used for the iterative algorithm (scaled units).

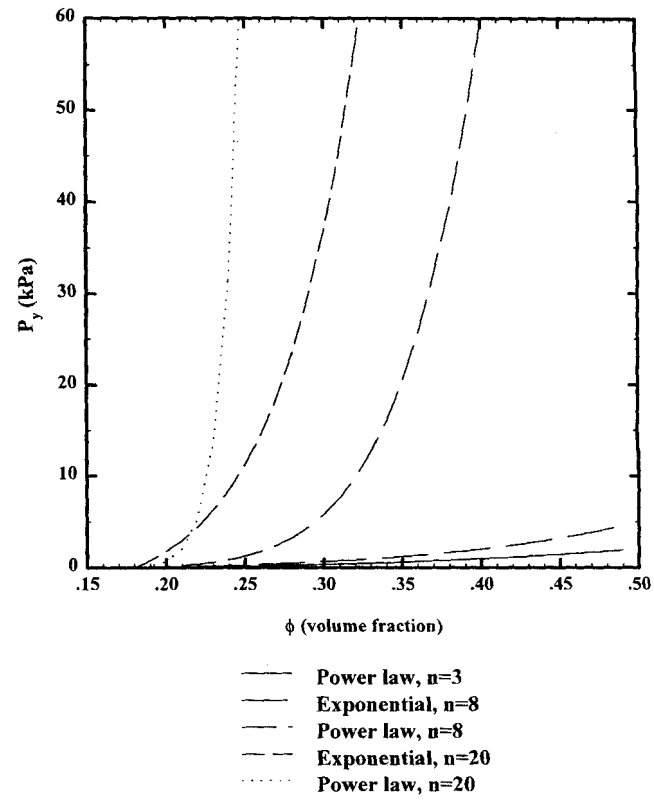

Figure 5. Synthetic compressive yield stress data used for validation of the algorithm.

scribed by Buscall and White (1987). The previously reported algorithm required two derivatives to be determined, namely dZ/dg as well as $d\Delta/dg$, which is essentially equivalent to finding d^2H_{eq}/dg^2 as well as dH_{eq}/dg. This earlier algorithm was used for some time (De Guingand, 1986; Green and Boger, 1992), but has less rigor and is unstable compared with the new technique described above. The new algorithm described here involves only one curve fit of the raw data and only one numerical differentiation, thus minimizing computational errors and enhancing stability.

Evaluation

To test the algorithm, two types of functions for $P_y(\phi)$ were used:

(1) A power law of the form $P_y(\phi) = A[(\phi/\phi_g)^n - 1]$

(2) An exponential of the form $P_y(\phi) = A[e^{n\phi} - e^{n\phi_g}]$

where A and n are constants. The precise forms of the functions used for various values of n are shown in Figure 5. These curves represent a wide range in the compression behavior of suspensions, although the power law curve of order 8 is the most realistic, being based on experimental data. The suspension characteristics used for all the curves were based on experimental results. The values used were $\phi_0 = 0.194$, $H_0 = 88.5$ mm, $\Delta\rho = 1{,}210$ kg/m^3, and $R = 155.8$ mm. From these $P_y(\phi)$ functions, synthetic (g, H_{eq}) data sets were generated by solving the main differential Eq. 4, using $P = P_y(\phi)$ in the compression region, and with appropriate boundary conditions. An example of the form of the synthetic data generated from an 8th-order power law function is given in Figure 6. These synthetic data sets were then run through the algorithm and the generated $P_y(\phi)$ curves were compared with the original exact solution in order to determine the algorithm's performance.

In order to model real experimental data, only a limited number of these generated (g, H_{eq}) points (7) were used. The number and spacing of the points that were chosen are typical of those used in laboratory experiments. It is only practical to obtain between 5 and 10 data points to build up a curve over the usual g range measured. For each experiment, the time to reach equilibrium for any particular speed can range from several days to over a week at the lower

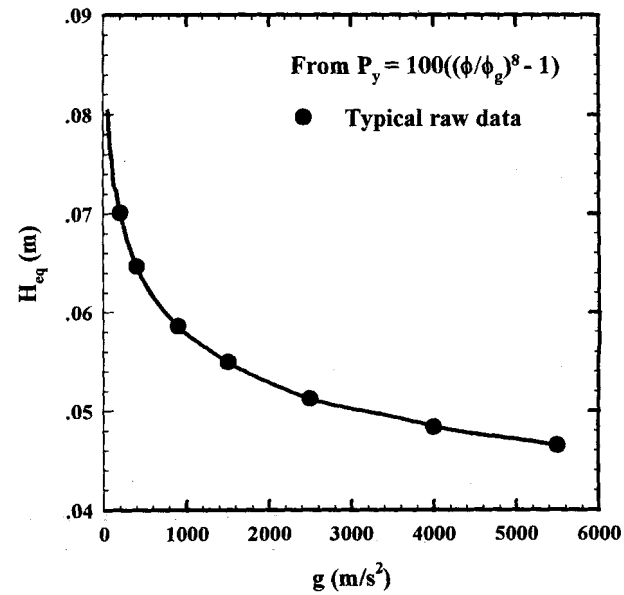

Figure 6. Typical raw data generated from an 8th-order power law function.

speeds, depending on the suspension and the initial concentration, and thus a complete run can take weeks. The spacing of the points is roughly logarithmic with g since the change in H_{eq} at lower g is greater. The points used for the 8th-order power law function are shown in Figure 6.

One of the dominant factors determining the accuracy of the solution was found to be the type of curve fitting used on the raw H_{eq} vs. g data. Curve fitting is necessary because, as noted, typically only a small number of data points will be known. The curve fit is critical since it is used to determine the derivative dH_{eq}/dg at each point, and the accuracy of this is strongly dependent on the goodness of the curve fit. This derivative is used in the equations for calculating ϵ and $\phi(0)$. The curve fitting used therefore affects both the approximate solution and the iterative solution to a similar degree by shifting the curve either to the left or to the right and has no effect on the calculated $P(0)$.

Several different curve fitting techniques were evaluated. These included polynomial fits of the order 1 through 5 and a generalized cross validation technique (Craven and Wahba, 1979) that optimizes the fit between a spline and a polynomial of any order. Both these techniques were tried using normal and logarithmic coordinates. The results for several of the better curve fits are compared against the exact solution in Figures 7 and 8. In general, the best solutions were found to be for second- or third-order polynomials fitted on logarithmic coordinates. The equations for these curve fits are of the general form

$$\ln H_{eq} = a_1 + a_2 \ln g + a_3(\ln g)^2 + a_4(\ln g)^3 + \ldots \quad (21)$$

where a_1, a_2, a_3, etc. are constants. The use of higher-order fits or of substantial splining were found to make the $P_y(\phi)$ curve oscillate about the true solution and thus should not be used, although they are useful in some circumstances when other curve fitting fails. The fitted curve must be as smooth as possible and must be a monotonically decreasing function

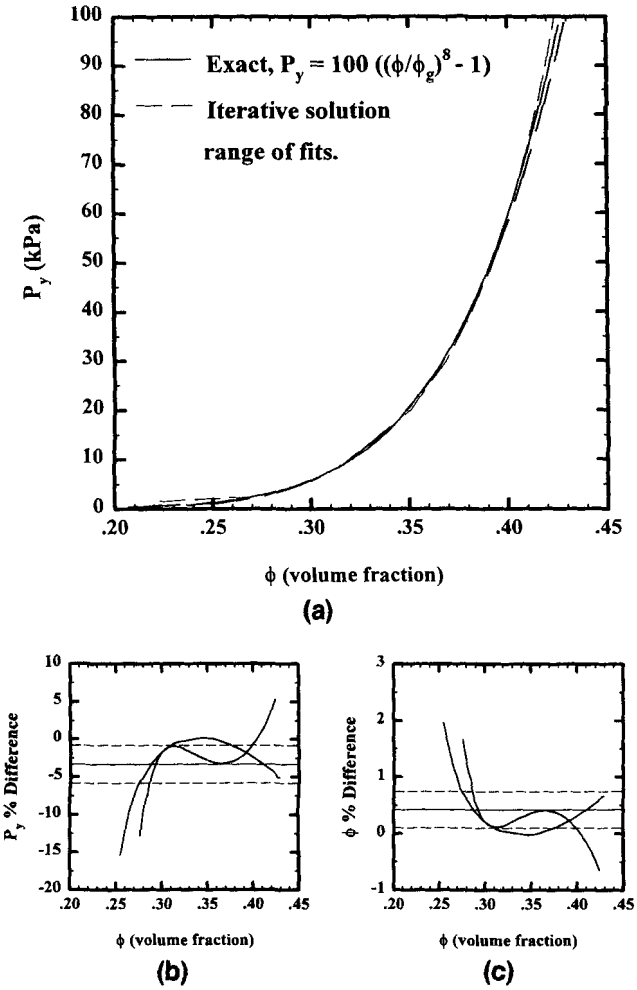

Figure 7. Comparison of the exact solution (8th-order power law) with that generated using the iterative solution.

(a) 2nd and 3rd order fits; (b) and (c) the % difference from the exact curve of P_y and ϕ respectively (also shown are the mean differences and the 99% confidence intervals).

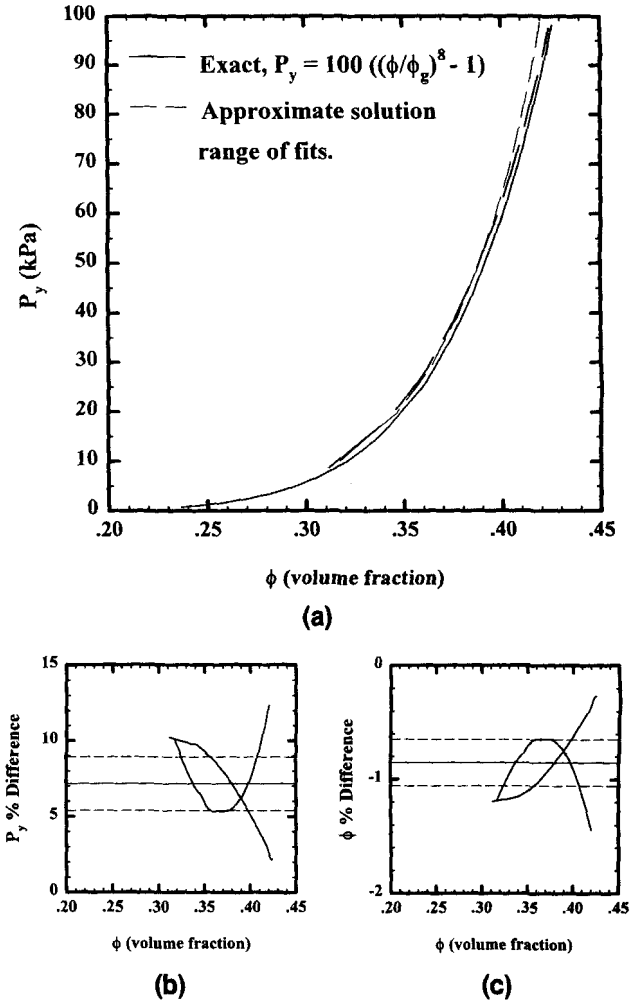

Figure 8. Comparison of the exact solution (8th-order power law) with that generated using the approximate solution.

(a) 2nd- and 3rd-order fits; (b) and (c) the % difference from the exact curve of P_y and ϕ respectively (also shown are the mean differences and the 99% confidence intervals).

with increasing g. In all cases, it is essential that the curve fitting results are viewed visually in order to determine whether or not they are satisfactory.

The accuracy of the iterative solution for all the data tested was generally very good. Shown in Figure 7 are the percentage differences between the iterative solution and the exact solution for the parameters ϕ and P_y for second- and third-order logarithmic curve fits of an 8th-order power law function. The solution tended to deviate from the exact solution at both high and low g or ϕ in each case, but the average of the different curve fits used was very close to the predicted curve. The error at the low end is due to extrapolation. The average error for ϕ was less than 0.5%, while the average error for P_y was about 5%, this being amplified by the error in ϕ due the power law nature of the curve. The error for the other curves tested was similar to that shown for this example. For a fuller analysis of the raw data, several of the best curve fits should thus be used and the results averaged in order to determine the best $P_y(\phi)$ curve.

The approximate solution was then compared to that determined by iteration. For all the types of curve fitting used, the approximate solution always underestimated the concentration $\phi(0)$, thus shifting the curve away from the true solution to lower ϕ. The largest shift always occurred for higher values of g (large ϕ), with the approximate curve lying closer to the iterative curve at the lower ϕ. In Figure 8, the corresponding approximate solution for the same data used in Figure 7 is shown. Here the difference between the approximate solution and the exact solution for various curve fits in terms of ϕ was less than 1%, about twice the error associated with the iterative solution. The error in P_y, as a result, ranged from +5–10%. In general, the iterative solution is thus more accurate than the approximate solution, as expected.

To simulate the effect of experimental error, random noise was added to the H_{eq} vs. g test data. Noise levels from 1 to 10% were applied to the H_{eq} data. The g data was assumed to contain no error. Typical values for the percentage error of H_{eq} for mineral suspensions studied at the University of Melbourne are less than 2%. Shown in Figure 9 are the results for the iterative solution on data containing 2% noise (data generated from the 8th-order power law). Even though the variation from the exact values is now larger, again especially for high g values, the average of the iterative solution for various different sets of "noisy" input data is close to the exact value. In order to minimize this sort of random error, several centrifuge tubes of the same sample should be run together and the resulting $P_y(\phi)$ curves averaged.

The error due to experimental error or noise should now be compared with the error associated with using the iterative and the approximate solution. This is crucial since it determines whether or not it is actually worthwhile to use the full iterative solution. Comparing Figures 7, 8, and 9, the variation in the $P_y(\phi)$ curves produced due to the noise is greater than that associated with both methods of solution. Therefore, if multiple runs cannot be made to minimize this random noise, the approximate solution may as well be used. The iterative solution, however, is still more accurate and, if available, will always give a more reliable result. The approximate solution, though, is perfectly suited to establish general trends in any particular system if absolutely correct values are not essential.

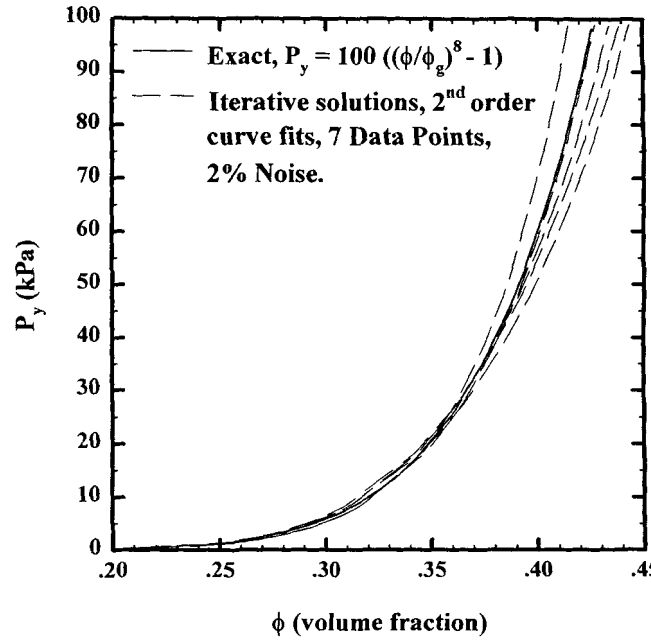

Figure 9. Examples of the effect of 2% noise on the iterative solution compared to the exact solution (8th-order power law).

In addition to errors in the measurement of H_{eq}, other errors also affect the accuracy of the compressive yield stress curve. Errors in the measurement of the initial concentration ϕ_0 and the initial height H_0 are directly translated to the error in both $\phi(0)$ and $P(0)$. The error in the density difference $\Delta\rho$ is also directly translated to the error in $P(0)$. The effect of the error in the centrifuge radius R is more complicated and affects both $\phi(0)$ and $P(0)$ but should be relatively small in most cases since this can be measured relatively accurately. However, at low speeds, when the carriers holding the centrifuge tubes are not horizontal, an angled sediment interface is formed. This can be accounted for by taking an average sediment height across the tube. Sometimes, it is not possible to use flat bottomed tubes if high speeds and/or high concentrations are required; instead, round bottomed tubes are used for strength considerations. The consolidation in the lower region of the tube is therefore nonlinear. An average centrifuge radius must then be used to account for this curvature which will have a larger associated error. All of these errors mentioned here must be considered when the results generated using the described iterative technique are evaluated. These error sources will also affect the results generated from the approximate solution in exactly the same way.

The equilibrium concentration and pressure profiles in the suspension $\phi(z)$ and $P(z)$ for each g point are calculated as part of the iterative algorithm. These profiles may be compared with those predicted by the exact solution. The theoretical profiles are generated in the production of the synthetic H_{eq} vs. g data. Figure 10 shows a selected set of these concentration profiles for the 8th-order power law synthetic data set overlaid on those produced by the algorithm. Agreement is generally very good which further validates the results. It can be seen from this plot that the concentration drops off steeply as $z \rightarrow z_c$ at medium to high g.

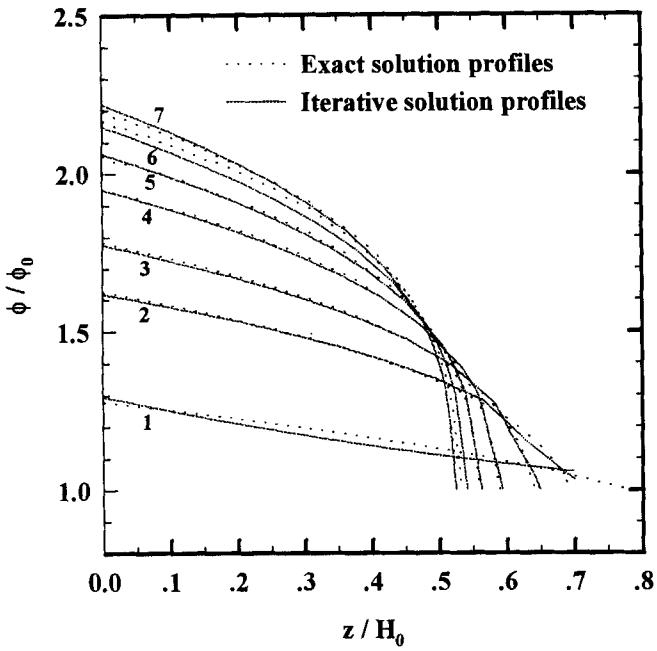

Figure 10. Comparison of the theoretical and the calculated concentration profiles (8th-order power law) for a selected number of g values.

(1) 76 m/s^2; (2) 520 m/s^2; (3) 1,076 m/s^2; (4) 2,187 m/s^2; (5) 3,298 m/s^2; (6) 4,964 m/s^2; (7) 5,520 m/s^2.

The calculated critical height z_c, the interface between the constant concentration region and the collapsing region, may also be compared with the theoretical z_c at each g. In Figure 11, this is shown for the 8th-order power law results. Also shown is the corresponding H_{eq} curve. The difference between the theoretical and the calculated z_c curves is not shown since agreement is again very good.

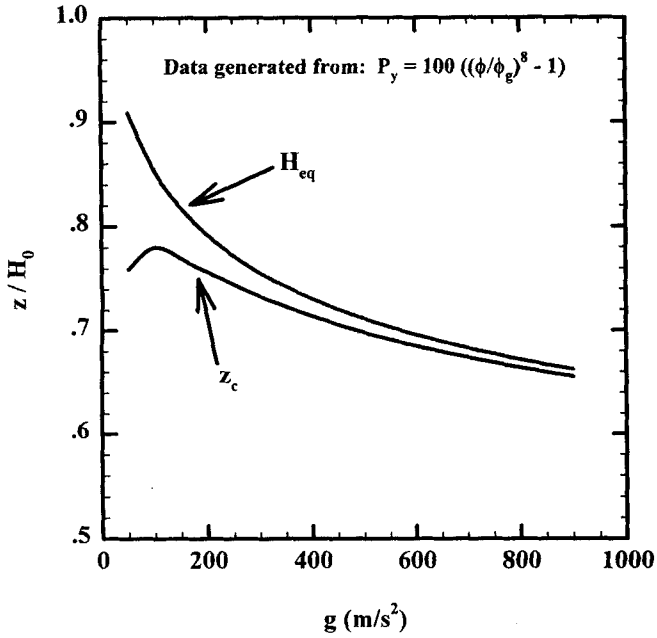

Figure 11. Typical behavior of H_{eq} and z_c with g (8th-order power law).

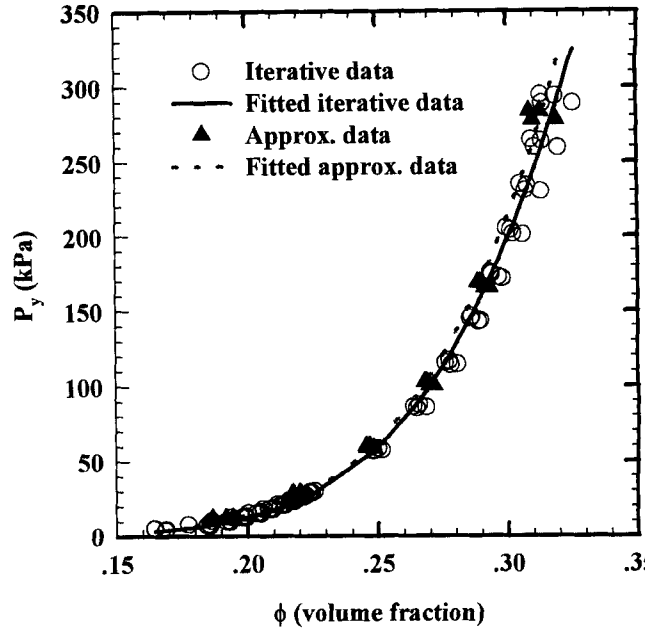

Figure 12. Example of experimental data: ZrO_2 aqueous suspension at pH 6.9, close to maximum flocculation.

Shown are the results from two samples each fitted by 2nd- and 3rd-order fits with the resulting data fitted with a line of best fit. The difference between the iterative and the approximate solutions is demonstrated.

Application

An example of how the iterative and the approximate algorithms may be used for real experimental data is shown in Figure 12. A ZrO_2 suspension at pH 6.9, close to its maximum flocculation condition, has been tested in two separate centrifuge tubes. The (g, H_{eq}) data from both samples have been analyzed using both 2nd- and 3rd-order logarithmic curve fits. The full iterative scheme was implemented, and the resulting $P_y(\phi)$ data points have been fitted with a curve of best fit. Similarly, the approximate scheme was implemented, giving rise to a second curve of best fit. It can be seen that the spread of the iterative and the approximate solution points is considerable and in fact overlap. The fit of the solution points indicate, as found for the synthetic data, that the approximate solution is shifted towards the left. The iterative solution should thus be a more accurate determination of the real compressive yield stress curve and should be used if multiple data sets are available.

Conclusions

The compressive yield stress $P_y(\phi)$ is a good measure of the network strength of flocculated suspensions. This parameter is used to characterize the compressional behavior of any particular suspension system and can be used in the design and operation of thickening and filtration process operations. An accepted engineering technique for the determination of the $P_y(\phi)$ function is the equilibrium sediment height technique in a centrifuge. Conversion of the raw data from this experiment to generate the $P_y(\phi)$ curve, however, is not a trivial exercise.

A new algorithm for the computation of the $P_y(\phi)$ curve has been determined. Results from a previously used algorithm have proved to be unstable. The new algorithm uses an iterative solution and is detailed here together with the approximate solution which uses the mean value theorem. From a detailed evaluation of both of these solution techniques using synthetically generated data, a number of main conclusions can be made.

- It can now be said with confidence that the equilibrium sediment height technique is valid for the determination of the compressive yield stress.
- In general, the iterative solution is more accurate than the approximate solution which tends to underestimate ϕ (up to approximately 2%).
- In most cases, satisfactory results can be obtained using the approximate solution, especially if only one set of raw data is available.
- Although the approximate solution has been used before, it is the first time that there has been justification for it and that its shortfalls have been quantified.
- The success of both the iterative and the approximate solutions rely heavily on the curve fitting method used on the raw data. For a fuller analysis, a number of curve fits to the (g, H_{eq}) raw data should be utilized and the resulting $P_y(\phi)$ curves averaged.

Acknowledgments

We would like to thank Professor Lee White for assisting with the development of the mathematical framework of the new algorithm. This research has been supported by the Advanced Mineral Products Centre at the University of Melbourne, a Special Research Centre of the Australian Research Council.

Literature Cited

Bergström, L., C. H. Schilling, and I. A. Aksay, "Consolidation Behaviour of Flocculated Alumina Suspensions," *J. Amer. Ceram. Soc.*, **75**(12), 3305 (1992a).

Bergström, L., "Sedimentation of Flocculated Alumina Suspensions: γ-ray Measurements and Comparison with Model Predictions," *J. Chem. Soc. Faraday Trans.*, **88**, 3201 (1992b).

Buscall, R., I. J. McGowan, P. D. A. Mills, R. F. Stewart, D. Sutton, L. R. White, and G. E. Yates, "The Rheology of Strongly-Flocculated Suspensions," *J. Non-Newt. Fluid Mech.*, **24**, 183 (1987).

Buscall, R., and L. R. White, "On the Consolidation of Concentrated Suspensions I: The Theory of Sedimentation," *J. Chem. Soc. Faraday Trans.*, **83**, 873 (1987).

Coe, H. S., and G. H. Clevenger, "Methods for Determining the Capacities of Slime-Settling Tanks," *Trans. Amer. Inst. Mining Engrs.*, **55**, 356 (1916).

Craven, P., and G. Wahba, "Smoothing Noisy Data with Spline Functions," *Num. Mathematik*, **31**, 377 (1979).

De Guingand, N. J., "The Behaviour of Flocculated Suspensions in Compression," Thesis (M.Eng.), University of Melbourne, Australia (1986).

Dixon, D. C., "Momentum-Balance Aspects of Free-Settling Theory: III. Transient Compression Resistance," *Sep. Sci. Tech.*, **13**, 753 (1978).

Eberl, M., K. A. Landman, and L. R. White, "Scale-Up Procedures and Test Methods in Filtration: a Test Case on Kaolin Plant Data," *Coll. Surf.*, **103**, 1 (1995).

Green, M. D., and D. V. Boger, "The Compressive Yield Stress of Zirconia Suspensions," *Proc. of the VIth Nat. Conf. on Rheology*, Clayton, Australia, p. 33 (1992).

Green, M. D., N. J. De Guingand, Q. D. Nguyen, and D. V. Boger, "The Shear and Compression Rheology of Bauxite Residue—An Overview," *Int. Bauxite Tailings Workshop*, Perth, Australia, p. 116 (1992).

Kos, P., "Fundamentals of Gravity Thickening," *Chem. Eng. Prog.*, **73**, 99 (1977).

Landman, K. A., L. R. White, and R. Buscall, "The Continuous-Flow Gravity Thickener: Steady State Behaviour," *AIChE J.*, **34**, 239 (1988).

Landman, K. A., L. R. White, and M. Eberl, "Pressure Filtration of Flocculated Suspensions," *AIChE J.*, **41**, 1687 (1995).

Michaels, A. S., and J. C. Bolger, "Settling Rates and Sediment Volumes of Flocculated Kaolin Suspension," *I&EC Fund.*, **1**, 24 (1962).

Miller, K. T., R. M. Melant, and C. F. Zukoski, "Comparison of the Compressive Yield Response of Aggregated Suspensions: Pressure Filtration, Centrifugation and Osmotic Consolidation," submitted to *J. Amer. Ceram. Soc.*, in press (1996).

Tadros, Th. F., "Rheology of Concentrated Suspensions," *Chem. Ind.*, 210 (April, 1985).

Tadros, Th. F., "Control of the Properties of Suspensions," *Coll. Surf.*, **18**, 137 (1986).

Appendix

Equation 4 can be rewritten as

$$\Delta\rho g\int_0^{H_{eq}}\phi\,dz=\int_0^{P(0)}\frac{dP}{1-z/R}. \tag{A1}$$

Using conservation of mass

$$\int_0^{H_{eq}}\phi\,dz=\phi_0 H_0, \tag{A2}$$

with Eq. A1 gives

$$\Delta\rho g\phi_0 H_0=\int_0^{P(0)}\frac{dP}{1-z/R}. \tag{A3}$$

Differentiating this equation with respect to g, noting that both z and $P(0)$ are functions of g, and rearranging gives

$$\frac{dP(0)}{dg}=\Delta\rho\phi_0 H_0-\frac{1}{R}\int_0^{P(0)}\frac{dP}{(1-z/R)^2}\frac{dz}{dg}. \tag{A4}$$

An alternate integration of Eq. 4 gives

$$\int_0^{P(z)}\frac{dP}{\phi(P)}=\Delta\rho g Z(z), \tag{A5}$$

where $Z(z)$ is defined as

$$Z(z)=\int_z^{H_{eq}}\left(1-\frac{z}{R}\right)dz=(H_{eq}-z)\left(1-\frac{H_{eq}+z}{2R}\right). \tag{A6}$$

For fixed $P(z)$, the lefthand side of Eq. A5 is fixed so that differentiating that equation with respect to g gives

$$0=Z(z)+g\frac{dZ}{dg}, \tag{A7}$$

and using the definition of $Z(z)$, this produces

$$\frac{dZ}{dg}=\left(1-\frac{H_{eq}}{R}\right)\frac{dH_{eq}}{dg}-\left(1-\frac{z}{R}\right)\frac{dz}{dg}, \tag{A8}$$

for fixed $P(z)$. This can be rewritten as

$$g\frac{dz}{dg}=\frac{Z(z)+\left(1-\frac{H_{eq}}{R}\right)g\frac{dH_{eq}}{dg}}{1-z/R}. \tag{A9}$$

Hence, from Eq. A4

$$\frac{dP(0)}{dg}=\Delta\rho\phi_0H_0-\frac{1}{gR}\int_0^{P(0)}\frac{dP}{(1-z/R)^3}\times\left(Z(z)+\left(1-\frac{H_{eq}}{R}\right)g\frac{dH_{eq}}{dg}\right), \tag{A10}$$

which can be written as

$$\frac{dP(0)}{dg}=\Delta\rho\phi_0H_0(1-\epsilon), \tag{A11}$$

where ϵ is a function of g and is given by

$$\epsilon=\frac{1}{\Delta\rho\phi_0H_0gR}\int_0^{P(0)}\frac{dP}{(1-z/R)^3}\times\left(Z(z)+\left(1-\frac{H_{eq}}{R}\right)g\frac{dH_{eq}}{dg}\right), \tag{A12}$$

or by using Eq. 4

$$\epsilon=\frac{1}{\phi_0H_0R}\int_0^{H_{eq}}\frac{dz\,\phi(z)}{(1-z/R)^2}\left(Z(z)+\left(1-\frac{H_{eq}}{R}\right)g\frac{dH_{eq}}{dg}\right), \tag{A13}$$

since $P=P(0)$ at $z=0$ and $P=0$ at $z=H_{eq}$.

Now, differentiating Eq. A5 with respect to g and rearranging gives

$$\phi(0)=\frac{\frac{dP(0)}{dg}}{\Delta\rho\frac{d[gZ(0)]}{dg}}. \tag{A14}$$

Thus, substituting in Eq. A11

$$\phi(0)=\frac{\phi_0H_0(1-\epsilon)}{\frac{d[gZ(0)]}{dg}} \tag{A15}$$

$$\therefore\ \phi(0)=\frac{\phi_0H_0(1-\epsilon)}{\left(H_{eq}+g\frac{dH_{eq}}{dg}\right)\left(1-\frac{H_{eq}}{R}\right)+\frac{H_{eq}^2}{2R}}. \tag{A16}$$

In order to get an expression for $P(0)$, Eq. 4 is written as

$$\phi(z)=\frac{1}{\Delta\rho g}\frac{dP}{dZ}, \tag{A17}$$

using the definition for $Z(z)$ in Eq. A6. Integration using Eq. A2 gives

$$\int_0^{H_{eq}}\frac{dP}{dZ}dz=\Delta\rho g\phi_0H_0. \tag{A18}$$

Integrating this by parts and using the definition of $Z(z)$ gives

$$P(0)=\Delta\rho g\phi_0H_0(1-\Delta), \tag{A19}$$

where Δ is a function of g given by

$$\Delta=\frac{1}{R}\int_0^{H_{eq}}\frac{dzP(z)}{\Delta\rho g\phi_0H_0(1-z/R)^2}. \tag{A20}$$

Manuscript received Aug. 8, 1995, and revision received Nov. 27, 1995.